Journal of Materials Chemistry A

Accepted Manuscript

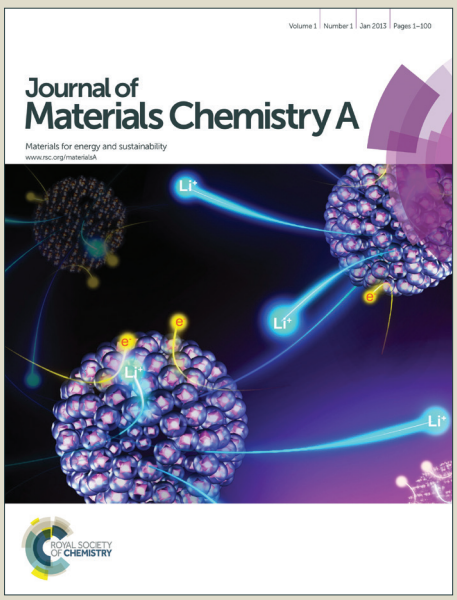

ROYAL SOCIETY OF CHEMISTRY

www.rsc.org/materialsA

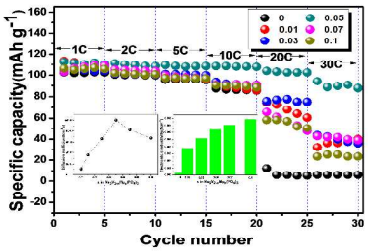

Mg doped $Na_3V_2(PO_4)_3$/C displays better electrochemical performance, especially at high rate. Enhanced rate capability and cycle performance can be attributed to the optimized particle size, structural stability and enhanced ionic and electronic conductivity induced by Mg doping.

Journal Name

RSCPublishing

ARTICLE

Effects of Mg Doping on Remarkably Enhanced Electrochemistry Performances of $Na_3V_2(PO_4)_3$ Cathode Material for Sodium Ion Batteries

Cite this: DOI: 10.1039/x0xx00000x

Received ooth January 2012,
Accepted ooth January 2012

DOI: 10.1039/x0xx00000x

www.rsc.org/

Hui Li,[a] Xiqian Yu,[b] Ying Bai,*[a] Feng Wu,[a] Chuan Wu,*[a] Liang-Yu Liu[a] and Xiao-Qing Yang*[b]

$Na_3V_{2-x}Mg_x(PO_4)_3$/C composites with different Mg^{2+} doping contents (x=0, 0.01, 0.03, 0.05, 0.07 and 0.1) were prepared by a facile sol-gel method. The doping effects on the crystal structure were investigated by XRD, XPS and EXAFS. The results show that low dose doping of Mg^{2+} does not alter the structure of the material, and magnesium is successfully substituted for vanadium site. The Mg doped $Na_3V_{2-x}Mg_x(PO_4)_3$/C composites exhibit significant improvements on the electrochemistry performances in terms of the rate capability and cycle performance, especially for the $Na_3V_{1.95}Mg_{0.05}(PO_4)_3$/C. For example, when the current density increased from 1 C to 30 C, the specific capacity only decreased from 112.5 mAh g^{-1} to 94.2 mAh g^{-1} showing very good rate capability. Moreover, even cycling at a high rate of 20 C, an excellent capacity retention of 81% is maintained from the initial value of 106.4 mAh g^{-1} to 86.2 mAh g^{-1} at the 50th cycle. Enhanced rate capability and cycle performance can be attributed to the optimized particle size, structural stability and enhanced ionic and electronic conductivity induced by Mg doping.

1 Introduction

In the past several decades, lithium ion batteries play an important role as the prominent power sources for electronic devices.[1-3] However, the limited abundance of lithium in the global scale, its uneven geographic distribution and difficulties in recycling lithium resources have raised concerns about large scale application of lithium ion batteries.[4-5] Therefore, the search for alternative energy-storage systems that could complement the existing lithium-ion batteries is getting more and more attention. Sodium, unlike lithium, is much more abundant on earth, where the sodium concentration is estimated to be 10320 ppm in seawater and 28300 ppm in the lithosphere.[6] In addition, sodium has similar physical and chemical properties as lithium. Therefore, the development of low-cost sodium ion batteries for large-scale energy storage system applications is very important.[7]

Recently, sodium ion batteries gained increasing attention due to their abundant reserves and relatively even geological distribution.[8] Actually, many electrode materials such as, $Na_4Fe_3(PO_4)_2(P_2O_7)$,[9] $Na[Ni_{0.25}Fe_{0.5}Mn_{0.25}]O_2$/C,[10] $Na[Li_{0.05}(Ni_{0.25}Fe_{0.25}Mn_{0.5})_{0.95}]O_2$,[11] $NaxCoO_2$,[12] $Na_2C_8H_4O_4$,[13] $Na_3(VO_{1-x}PO_4)_2F_{1+2x}$,[14] Prussian Blue analogues,[15,16] Phosphorus,[17,18] TiO_2[19] have been studied as active materials in

cathodes and anodes for sodium ion batteries. However, due to the bigger ionic radius of the sodium ion than lithium ion (1.02Å for Na^+ vs 0.76Å for Li^+), their storage performance and cycle performance are much poorer than their lithium counterparts. The larger Na^+ ionic radius is proved to be a crucial obstacle for Na^+ diffusion.[20,21] Therefore, improving the Na^+ diffusion is quite important in developing new electrode materials for sodium-ion batteries with good electrochemical performance.

NASICON-type $Na_3V_2(PO_4)_3$ has recently been investigated as a prospective cathode material for sodium ion batteries. It is worth noting that $Na_3V_2(PO_4)_3$ possesses the highly covalent three dimensional framework that generates large interstitial spaces through which sodium ions may diffuse easily.[22-27] In addition, the electrochemical response of the $Na_3V_2(PO_4)_3$ electrode displays two flat plateaus at 3.4 V and 1.6 V *vs*. Na^+/Na; the voltage plateau located at 3.4 V is relatively higher than most of other cathode materials for sodium ion batteries in recent reports.[28,29] However, $Na_3V_2(PO_4)_3$ also has inherent deficiency. The distorted VO_6 octahedral units in the NASICON structure negatively affects the electronic conductivity, making the electronic conductivity of $Na_3V_2(PO_4)_3$ similar as $Li_3V_2(PO_4)_3$ and $LiFePO_4$, and significantly limits its electrochemical performance.[28-32]

Up to now, two major methods have been used to increase the electric conductivity of $Na_3V_2(PO_4)_3$: (i) coating various carbon materials;[25,30] (ii) reducing the particle size to nano-size.[24,31] The surface coated carbon mainly improves the electronic conductivity of $Na_3V_2(PO_4)_3$, and nanosized particles can improve ionic conductivity through shortening the diffusion distance of sodium ion. However, the bulk phase characteristic of $Na_3V_2(PO_4)_3$ is hard to be modified by these methods at all. On the other hand, doping foreign ion has been proved to be effective in improving the intrinsic electronic conductivity in lithium ion batteries.[32] Goodenough and co-workers[33] reported the improved charge-transfer kinetics of $LiFePO_4$ by anion site modifications with sulfur and nitrogen via density functional theory (DFT) calculations. Wang[34] demonstrated that the olivine phosphate, when co-modified with graphene and Mg^{2+} doping demonstrates improved kinetic properties. Although significant amount of results about doping various ions in electrode materials for lithium ion batteries have been reported, in contrast, similar reports for sodium ion batteries are much less in the literature, especially for $Na_3V_2(PO_4)_3$ electrode material.

In this work, Mg was selected to dope $Na_3V_2(PO_4)_3$/C cathode material, due to the light atomic weight and the advantages for improving performances of the electrode materials revealed in lithium ion batteries. Comparing with undoped $Na_3V_2(PO_4)_3$/C, the Mg doped $Na_3V_{2-x}Mg_x(PO_4)_3$/C composites exhibit remarkable improvements in Na storage performances, in terms of the rate capability and cyclic stability. The effects of Mg doping on modification of the crystal structure and the electric properties of the doped materials are explored in detail, with the interpretion of the enhanced electrochemical performance in this paper.

2 Experimental Section

2.1 Materials Preparation

The $Na_3V_{2-x}Mg_x(PO_4)_3$/C samples, where x=0, 0.01, 0.03, 0.05, 0.07 and 0.1, were synthesized by a sol-gel method using NaOH, NH_4VO_3, $NH_4H_2PO_4$, $Mg(CH_3COO)_2$ and citric acid as starting materials. Citric acid was used as both chelating reagent and carbon source. Firstly, citric acid was dissolved in deionized water with continuous stirring at room temperature. Then, after a clear solution was formed, a mixture of stoichiometric NaOH, NH_4VO_3, $Mg(CH_3COO)_2$ and $NH_4H_2PO_4$(3.1:2-x:x:3,x=0,0.01,0.03,0.05,0.07 and 0.1) was added to the solution with violently stirring, and then a gel formed at 80 ^oC. The gel was initially heated to 350 ^oC in air atmosphere for 4 h, followed by cooling to room temperature. Finally, the obtained product was slightly ground and reheated

at 800 °C for 8 h under flowing argon to yield the $Na_3V_{2-x}Mg_x(PO_4)_3$/C. All chemical reagents were of analytical grade and used as received without any further purification.

2.2 Characterizations

X-ray diffraction (XRD) characterization was performed using an X-ray diffractometer (D/MAX-RB) with a Cu Ka radiation at ambient temperature. The chemical compositions of the synthesized powders were determined using inductively coupled plasma optical emission spectrometer (ICP-OES, IRIS Intrepid II XSP). The surface morphology of the sample was observed by scanning electron microscopy(SEM, HITACHI S-4800). The Raman spectra were taken by using a lab RAM ARAMIS laser Raman spectroscopy equipped with a 514 nm Ar-ion laser. The HRTEM images were obtained using a high-resolution transmission electron microscope (Hitachi H-800). The carbon content of the sample was obtained by using an organic element analyzer (Vario EL cube). X-ray photoelectron spectroscopy (XPS) (PHI5700, America) with monochromatic Al Ka radiation was employed to investigate the oxidation state of V in the $Na_3V_{2-x}Mg_x(PO_4)_3$/C samples. The binding energy values were calibrated by using the value of carbon contaminant on the sample (C1s = 284.5 eV) as a reference. X-ray absorption spectroscopy (XAS) experiments were carried out at beamline 9-BM-B (APS, ANL) in transmission mode using a Si (111) double-crystal monochromator detuned to the 50% value of its original maximum intensity to eliminate the high order harmonics. X-ray absorption near edge structure (XANES) and extended X-ray absorption fine structure (EXAFS) data were analyzed by ATHENA software package.[35]

2.3 Electrochemical tests

The electrochemical tests were carried out using coin cells (CR2025) assembled in an argon filled glove box (Labmaster130). The cathode electrodes consist of 80 wt % active material, 10 wt % SP, and 10 wt % polyvinylidene fluoride (PVDF) binder. The mixed slurry was spread onto aluminum foil. Then, the electrodes were dried at 80 °C over 8 h to remove the solvent before pressing. Then a circular cathode disc with a diameter of 1.0 cm was punched from the aluminum foil. The mass loading of the active material was typically around 2.3 mg cm^{-2}. The cell was made using sodium metal foil as the anode and Celgard 2400 as separator. The electrolyte was 0.6 M $NaPF_6$ in a mixture of ethyl carbonate (EC) and diethyl carbonate (DEC) (volume ratio=1:1). Galvanostatic discharge/charge measurements were carried out in LAND battery test system (CT2001A, Wuhan, China) in the potential range of 2.5-4.0 V (*vs*. Na^+/Na) under various current densities. Before the charge/discharge tests, the batteries were aged for 10 h to ensure good soakage of the $Na_3V_{2-x}Mg_x(PO_4)_3$/C(x=0, 0.01, 0.03, 0.05, 0.07 and 0.1) in the cathode by the electrolyte. To evaluate the Na^+ diffusion coefficient, electrochemical impedance spectroscopy (EIS) was performed on an electrochemical workstation (CHI 660a, Shanghai, China), over a frequency range of 100 kHz to 10 mHz with an applied amplitude of 5 mV. The parameters of the equivalent circuit were calculated and analyzed by computer simulations using the ZView software. The electronic conductivity measurements were performed on a RTS-4 linear four-point probe system. Firstly, 1 g $Na_3V_{2-x}Mg_x(PO_4)_3$/C(x=0, 0.01, 0.03, 0.05, 0.07 and 0.1) without any adhesives was placed in a powder tablet machine with the pressure of 10 Mpa to make the $Na_3V_{2-x}Mg_x(PO_4)_3$/C(x=0, 0.01, 0.03, 0.05, 0.07 and 0.1) pellet, respectively. Then, for each sample, the electronic conductivity was measured at five different positions on the $Na_3V_{2-x}Mg_x(PO_4)_3$/C(x=0, 0.01, 0.03, 0.05, 0.07 and 0.1) pellet with 15mm in diameter and 1 mm in thickness to calculate the average electronic conductivity value.

Journal Name RSCPublishing

ARTICLE

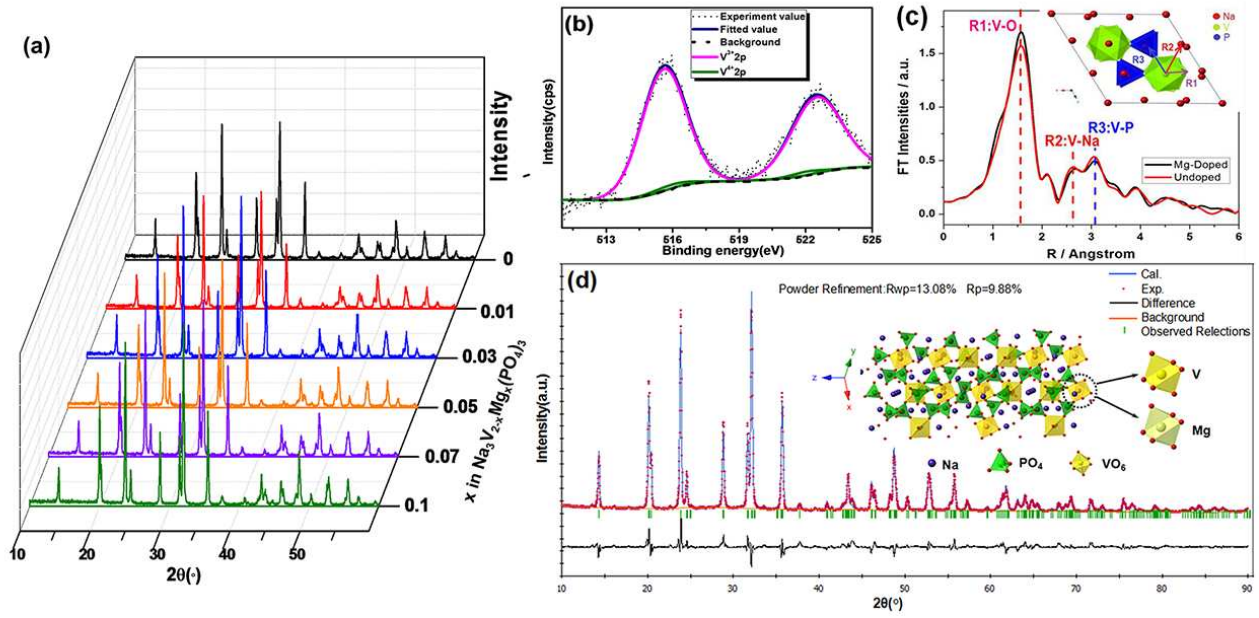

Fig. 1 a) XRD patterns of $Na_3V_{2-x}Mg_x(PO_4)_3$ phases (x = 0.00, 0.01, 0.03, 0.05, 0.07 and 0.1). b) X-ray photoelectron spectroscopy of V_{2p} in $Na_3V_{1.95}Mg_{0.05}(PO_4)_3$. c) EXAFS spectra of undoped and Mg doped $Na_3V_2(PO_4)_3$. d) Rietveld refined XRD patterns of $Na_3V_{1.95}Mg_{0.05}(PO_4)_3$.

3 Results and discussion

In order to confirm the effects of Mg^{2+} doping on the structure of $Na_3V_2(PO_4)_3$, XRD patterns for a series of Mg doped $Na_3V_2(PO_4)_3$ were collected and the results are shown in Fig. 1a. All of the diffraction peaks can be assigned to the NASICON structure with $R\bar{3}C$ space group (2 Na in 18e position, 1 Na in 6b position). No Bragg peaks representing impurities or other structures have been detected, indicating that low dose doping of Mg^{2+} does not alter the structure of the material.

According to the reports about ion doping in lithium transition metal phosphates materials for lithium ion batteries, there are two available sites for ion doping. One is lithium site, and the another is transition metal site.[36,37] To identify the doping site of Mg in $Na_3V_{2-x}Mg_x(PO_4)_3$, X-ray photoelectron spectroscopy (XPS) was used to study the oxidation states of the vanadium in the compounds with x= 0.05 to further identify the doping site of Mg. Replacing V^{3+} with Mg^{2+}, due to the different valence state between V^{3+} and Mg^{2+}, will lead to the formation of V^{4+}. Fig. 1b illustrates the experimental values and the fitted curves of XPS for V_{2p}. The fitting results are given in Table S1. The scale of binding energy (BE) is referenced by setting the BE of C1s to 284.5 eV. As can be seen from Fig. 1b, the V $2p_{3/2}$ fits to peaks with the BE of 515.5 eV and 515.8 eV, which match well with those measured in V_2O_3 (515.3 eV) and VO_2 (515.75 eV) in the literature.[38,39] Therefore, it is reasonable to assume that both the V^{3+} and V^{4+} ion coexist in Mg doped $Na_3V_2(PO_4)_3$ and magnesium is successfully substituted for vanadium as designed. To explore the effects of Mg^{2+} doping

on the structure of $Na_3V_2(PO_4)_3$, the extended X-ray absorption fine structure (EXAFS) spectra analysis was performed to investigate the local environment around V (Fig. 1c). Each reflection peaks shown in the EXAFS spectra represents the interaction between V ions and the surrounding atoms as labeled on the inset figure of the crystal structure. The slight peak intensity differences between undoped and doped $Na_3V_2(PO_4)_3$ indicate slight local structure changes (e.g. disordered extent, vacancies etc.) occurring around V site upon Mg doping. The peak positions remain unchanged indicating that the crystal framework doesn't change with Mg doping. This is in good agreement with the XRD and XPS results on the successful substitution of magnesium at vanadium sites.

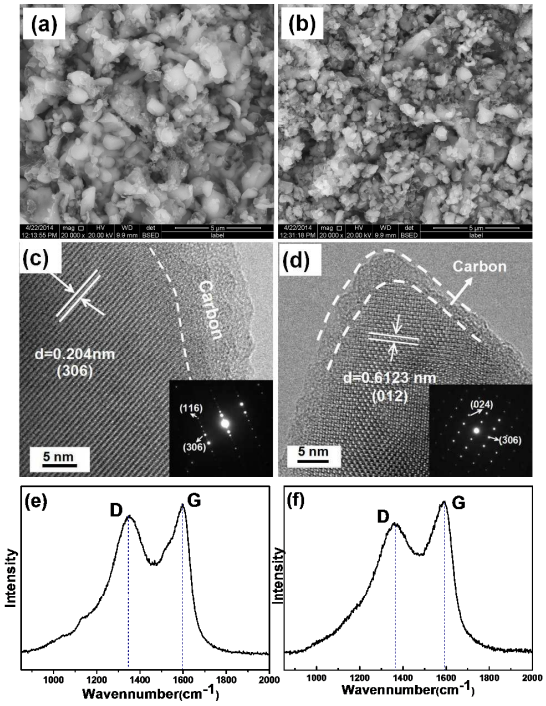

Fig. 2 a) SEM image of $Na_3V_2(PO_4)_3$/C. b) SEM image of $Na_3V_{1.95}Mg_{0.05}(PO_4)_3$/C. c) HRTEM image of $Na_3V_2(PO_4)_3$/C(inset:the selected-area electron diffraction (SAED) pattern of $Na_3V_2(PO_4)_3$/C). d) HRTEM image of $Na_3V_{1.95}Mg_{0.05}(PO_4)_3$/C (inset: the selected-area electron diffraction (SAED) pattern of $Na_3V_{1.95}Mg_{0.05}(PO_4)_3$/C). e) Raman spectrum of $Na_3V_2(PO_4)_3$/C. f) Raman spectrum of $Na_3V_{1.95}Mg_{0.05}(PO_4)_3$/C.

In order to further explore the structure change affected by the Mg doping, the Rietveld refinement was conducted for the $Na_3V_{2-x}Mg_x(PO_4)_3$ compounds with x = 0 (Fig. S1) and 0.05 (Fig. 1d). In this work, the refinements were carried out using the GSAS program suite, and a space group of $R\bar{3}C$ was chosen as the refinement model. The data of calculated lattice parameters are listed in Table S2-S4. The value of the "a" axis (a=b axis), "c" axis and the lattice volume decrease slightly with Mg^{2+} doping. It is in agreement with the fact that the radius of Mg^{2+} (r =0.65 Å) is smaller than that of V^{3+} (r =0.74 Å). In addition, the average lengths of the V–O and P–O bond for $Na_3V_{1.95}Mg_{0.05}(PO_4)_3$ is shorter than $Na_3V_2(PO_4)_3$, suggesting that the composites modified by Mg^{2+} doping have a more stable structure for the charge/discharge reaction.[34,40] Meanwhile, the shortened average bond of V–O and P–O may cause broadening of the channels for sodium ion diffusion. Moreover, the average length of the Na–O bond of $Na_3V_{1.95}Mg_{0.05}(PO_4)_3$/C is longer than $Na_3V_2(PO_4)_3$/C. A longer Na–O bond has a smaller binding energy, leading to an easy migration of Na^+ due to the reduction of the energy barrier, which will be beneficial to the electrochemical performance of cathode materials, especially at the high-C rate.[41.42]

To obtain the precise elemental compositions of the Mg^{2+} doping samples, the ICP-OES was employed. Table S5 lists the molar ratios of Na, V and Mg for the samples with different Mg^{2+} doping amounts. It has been found that the molar ratios are very close to the theoretical values, which implies that the V atoms were successfully replaced by Mg atoms, at different doping levels, as designed.

In order to confirm the effects of Mg^{2+} doping on the morphology of $Na_3V_2(PO_4)_3$, the undoped sample $Na_3V_2(PO_4)_3$

and $Na_3V_{2-x}Mg_x(PO_4)_3$/C(x=0.01, 0.03, 0.05, 0.07 and 0.1) composites were investigated by SEM. As can be seen in the SEM images, a severely aggregated morphology can be observed for $Na_3V_2(PO_4)_3$ sample in Fig. 2a, while the Mg doped samples have smaller particles sizes and narrower particles size distribution of 0.5-5.0 μm in Fig. 2b and Fig. S2. These results confirm that the Mg doping may slightly affect the morphology of samples. The reduced particle sizes for $Na_3V_{2-x}Mg_x(PO_4)_3$/C (x=0.01, 0.03, 0.05, 0.07 and 0.1) can be attributed to the decomposition of $Mg(CH_3COO)_2$ in the precursor mixtures, which prevents the agglomeration of final products during high temperature sintering.[43] The energy dispersive X-ray (EDX) elemental mapping results of $Na_3V_2(PO_4)_3$/C and $Na_3V_{1.95}Mg_{0.05}(PO_4)_3$/C are shown in Fig. S3. It is clearly seen that Na,V, P, O and Mg distributions were quite uniform in $Na_3V_{1.95}Mg_{0.05}(PO_4)_3$/C. To further investigate the morphology and microstructure of the various samples, HRTEM images of the $Na_3V_2(PO_4)_3$/C and $Na_3V_{1.95}Mg_{0.05}(PO_4)_3$/C particles are shown in Fig. 2c and 2d. As can be seen, both the $Na_3V_2(PO_4)_3$/C and $Na_3V_{1.95}Mg_{0.05}(PO_4)_3$/C are coated with uniform carbon layers on the particles surface. It has been proved that the carbon layer would result in the formation of a mixed conducting network, which is beneficial for both electron and ion transport.[24] Furthermore, the clear lattice fringes can be observed for these two samples. In Fig. 2c, the lattice fringes with a d-spacing of approximately 0.204 nm corresponds to the distance between (306) planes of $Na_3V_2(PO_4)_3$/C can be observed; Fig. 2d presents lattice fringes with a d-spacing of 0.6123 nm, which is in good agreement with that of the (012) planes for $Na_3V_{1.95}Mg_{0.05}(PO_4)_3$/C. The inset of Fig. 2c and 2d are selected-area electron diffraction (SAED) patterns indicating the highly ordered single-crystal character of these two samples.

In order to identify the nature of the carbon layer formed on the surface of particles, Raman spectra were recorded for both the pristine and $Na_3V_{1.95}Mg_{0.05}(PO_4)_3$/C powders and the results are given in Fig. 2 e-f. For both the $Na_3V_2(PO_4)_3$/C and $Na_3V_{1.95}Mg_{0.05}(PO_4)_3$/C samples, two distinguishable peaks at about 1360 cm^{-1} (D-band) and 1600 cm^{-1} (G-band) are obtained, indicating the existence of the carbon layer in the materials. In a little more detail, the frequency of ~1600 cm^{-1} corresponds to the G mode with the optically allowed E_{2g} vibrations of the graphitic structure was observed for both samples, showing that the carbon films coated on the particles are partially graphitized. On the other hand, the D mode band with characteristic frequency of ~ 1360 cm^{-1} relating to the disordered carbon was also observed.[44] The intensity ratio between D and G modes provides information about the degree of crystallinity of carbon layer. In the present case, the I_D/I_G ratio are 0.92 and 0.90 for $Na_3V_2(PO_4)_3$/C and $Na_3V_{1.95}Mg_{0.05}(PO_4)_3$/C, respectively, indicating that the coating predominantly contains sp^2 type carbon, thereby enabling good electronic conductivity profiles.[45] In addition, the carbon content of the various samples evaluated by organic elemental analysis was about 4.58 wt % and 4.23 wt % for $Na_3V_2(PO_4)_3$/C and $Na_3V_{1.95}Mg_{0.05}(PO_4)_3$/C, respectively. Due to the similar I_D/I_G ratio and carbon content, it can be concluded that the carbon layer plays an equally important role in the electrochemical performance for both $Na_3V_2(PO_4)_3$/C and $Na_3V_{1.95}Mg_{0.05}(PO_4)_3$/C.

The electrochemical performances of $Na_3V_{2-x}Mg_x(PO_4)_3$/C (x=0, 0.01, 0.03, 0.05, 0.07 and 0.1) cathodes were investigated in detail and presented in Fig. 3. To investigate the rate capability, the $Na_3V_{2-x}Mg_x(PO_4)_3$/C (x=0, 0.01, 0.03, 0.05, 0.07 and 0.1) were tested stepwise from 1 to 30 C and the results are shown in Fig. 3a (note that 1 C means the full capacity can be charged or discharged in 1 h and 1 C = 117.6 mA g^{-1} in this work). The discharge capacities of all Mg doped materials are

Journal Name RSCPublishing

ARTICLE

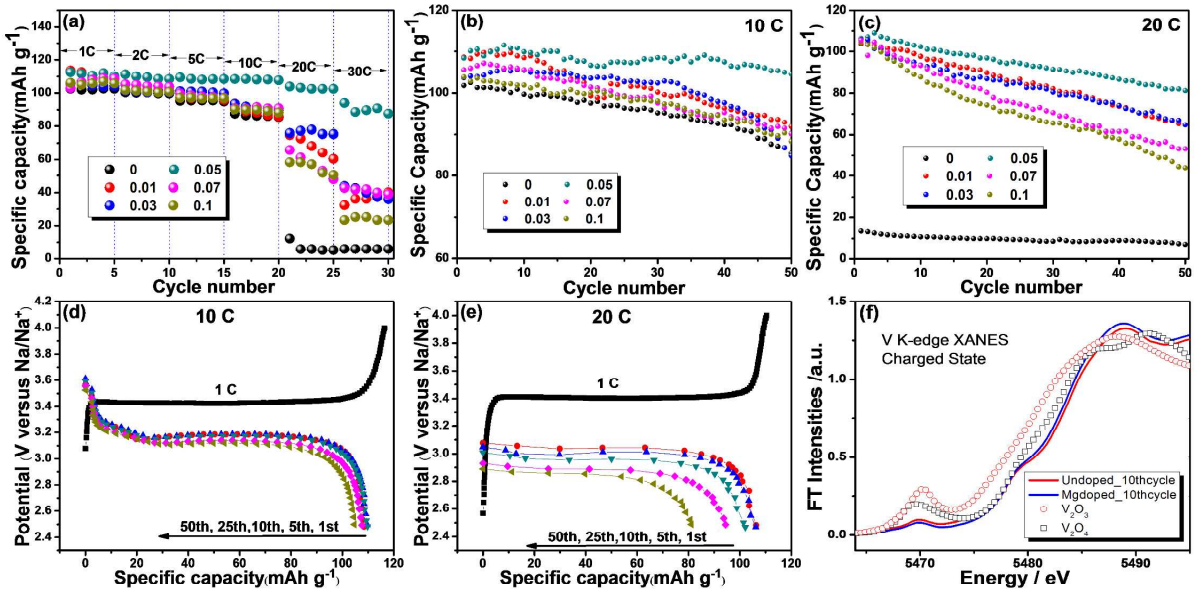

Fig. 3 a) Rate capability of $Na_3V_{2-x}Mg_x(PO_4)_3/C$(x=0, 0.01, 0.03, 0.05, 0.07 and 0.1) at different current densities. Cycling stability of $Na_3V_{2-x}Mg_x(PO_4)_3/C$(x=0, 0.01, 0.03, 0.05, 0.07 and 0.1) at b) 10 C and c) 20 C. Charge/discharge profiles of $Na_3V_{1.95}Mg_{0.05}(PO_4)_3/C$ at various cycles at current densities of d) 10 C and e) 20 C. f) X-ray absorption spectra at V K-edge for Undoped and Mg-doped $Na_3V_2(PO_4)_3$ collected at the charged state. Reference spectra of V_2O_3 and V_2O_4 standard materials were presented to identify the oxidization states of the investigated materials.

obviously better than the undoped one. The $Na_3V_{1.95}Mg_{0.05}(PO_4)_3/C$ sample shows the highest capacity. The discharge capacities of 102.6, 101.3, 97.2, 90.4, 5.8 and 5.9 mAh g^{-1} were obtained at 1, 2, 5, 10, 20 and 30 C for $Na_3V_2(PO_4)_3/C$, respectively. In contrast, $Na_3V_{1.95}Mg_{0.05}(PO_4)_3/C$ shows remarkably improved rate capability and delivers a discharge capacity as high as 112.5, 111.3, 109.9, 108.5, 103.9 and 94.2 mAh g^{-1} at 1, 2, 5, 10, 20 and 30 C. When the rate was increased from 1 C to 30 C, a high capacity retention of 83.7 % was obtained. Such excellent rate capability is also quite impressive when compared to the reported values in the literature (Table S6). In addition, it is worth noting that when all the samples cycled at current densities as high as 20 C and 30 C, the undoped $Na_3V_2(PO_4)_3/C$ can only deliver discharge capacity around 5 mAh g^{-1}, which can be considered that the $Na_3V_2(PO_4)_3$ electrode has lost the ability to charge/discharge. In comparison, the discharge capacities of Mg doped $Na_3V_{1.95}Mg_{0.05}(PO_4)_3/C$ can still reach up to 103.9 and 94.2 mAh g^{-1} at 20 C and 30 C, respectively. Therefore, it can be conclude that Mg doping in $Na_3V_2(PO_4)_3$ obviously enhance the rate capability, particularly at high rates. It is interesting to note that with the increasing Mg doping content, the discharge capacities under the same current densities increase first, reach a maximum value when the x is 0.05 in $Na_3V_{2-x}Mg_x(PO_4)_3/C$, then decrease (Fig. S4). A more detailed discussion about the reason for the volcano-type variation in the discharge capacity with doping level will be provided at the end of this paper.

Good high rate cycling is one of the most important electrochemical performance requirements of sodium ion batteries for the power storage application. A comparison of the discharge capacity as a function of cycle number for $Na_3V_{2-x}Mg_x(PO_4)_3$ with different Mg doping content (x = 0.00, 0.01, 0.03, 0.05, 0.70 and 0.1) are given in Fig. 3 b-c. The samples were cycled between 2.5 to 4.0 V at different discharge rates (10 C and 20 C). It is easy to find that Mg doped $Na_3V_2(PO_4)_3$ cathode materials exhibit better rate capability and long term cycle stability than the undoped one, both at 10 C and 20 C. As shown in Fig. 3b, $Na_3V_{1.95}Mg_{0.05}(PO_4)_3$ displays the best cycle performance: The initial capacity is 108.4 mAh g^{-1} at 10 C; after 50 cycles, it remained as high as 104.6 mAh g^{-1} with only 3.5 % lost. In contrast, the initial discharge capacity of $Na_3V_2(PO_4)_3$ sample was at a lower level of 101.8 mAh g^{-1}; after 50 cycles, only 85.5 mAh g^{-1} could be obtained with 16 % lost. At the higher rate of 20 C, such improvement in rate capability and cycle stability for Mg^{2+} doped samples(Fig. 3c) is much more significant: The $Na_3V_2(PO_4)_3$ can only deliver initial discharge capacity around 10 mAh g^{-1} at 20 C. In contrast, the $Na_3V_{1.95}Mg_{0.05}(PO_4)_3$ was able to deliver an impressive initial value of 106.4 mAh g^{-1} at the same rate and finally stabilized at 86.2 mAh g^{-1} after 50 cycles, demonstrating outstanding capacity retention. The excellent cycle stability of $Na_3V_{2-x}Mg_x(PO_4)_3$ is further confirmed by discharge curves at various cycles under 10 C and 20 C rates (Fig. 3 d-e). We can see that even during a prolonged cycling test on $Na_3V_{2-x}Mg_x(PO_4)_3$ electrode, there is nearly no apparent change in the charge=discharge profiles up to 50 cycles at 10 C. In Fig. 3d, the obvious discharging plateau is observed at 3.2 V in the first cycle, with only a little potential drop (0.1 V) during the charge/discharge process up to the 50th cycle. Even at the higher current density of 20 C (Fig. 3e), the quite flat plateaus also can be observed during the prolonged cycling test, suggesting the excellent reversible sodium ion battery performance, structure stability of Mg-doped $Na_3V_{2-x}Mg_x(PO_4)_3$.

In order to understand the Na storage mechanism of undoped and Mg doped $Na_3V_2(PO_4)_3$, V K-edge XAS spectra were collected to examine the oxidation states of V at the fully charged state. The corresponding X-ray absorption near edge spectroscopy (XANES) results are shown in Fig. 3f. It can be seen that at the fully charged state, the XANES edge features of both undoped and Mg doped $Na_3V_2(PO_4)_3$ resemble that of the reference standard material V_2O_4, indicating V ions have been oxidize to tetravalent state. Combining the charge/discharge profiles and XANES, we can deduce that the charge/discharge mechanism of Mg doped materials is similar with the undoped one, the sodium extraction/insertion behavior can be described with the following reactions:

$$Na_3V_2^{3+}(PO_4)_3 \Leftrightarrow NaV_2^{4+}(PO_4)_3 + 2Na^+ + 2e^- \quad (1)$$

$$Na_3V_{2-2x}^{3+}V_x^{4+}Mg_x(PO_4)_3 \Leftrightarrow Na_{1+2x}V_{2-x}^{4+}Mg_x(PO_4)_3 + (2-2x)Na^+ + (2-2x)e^- \quad (2)$$

where the reaction (1) and (2) correspond to the charge/discharge behavior of $Na_3V_2(PO_4)_3$ and $Na_3V_{2-x}Mg_x(PO_4)_3$/C, respectively.

Electrochemical impedance spectroscopy (EIS) was employed to investigate the electrode kinetics of various $Na_3V_{2-x}Mg_x(PO_4)_3$/C (x=0, 0.01, 0.03, 0.05, 0.07 and 0.1) samples. The Nyquist plots of the various $Na_3V_{2-x}Mg_x(PO_4)_3$/C (x=0, 0.01, 0.03, 0.05, 0.07 and 0.1) electrodes charged to 4 V after 4 cycles are depicted in Fig.4a. In the Nyquist plots, each impedance spectrum consists of a depressed semicircle at high frequency, and a slope line at the low frequency range. The semicircle in the high frequency region is attributed to charge transfer resistance. The straight line in the low frequency region represents the diffusion of the sodium ions into the bulk of electrode material.[46-48] The inset of Fig. 4a is the equivalent circuit used to fit the EIS. In the circuit, the small intercept depicts the bulk resistance of the cell (Rs); CPE represents the double layer capacitance and capacity of surface layer; and Rct

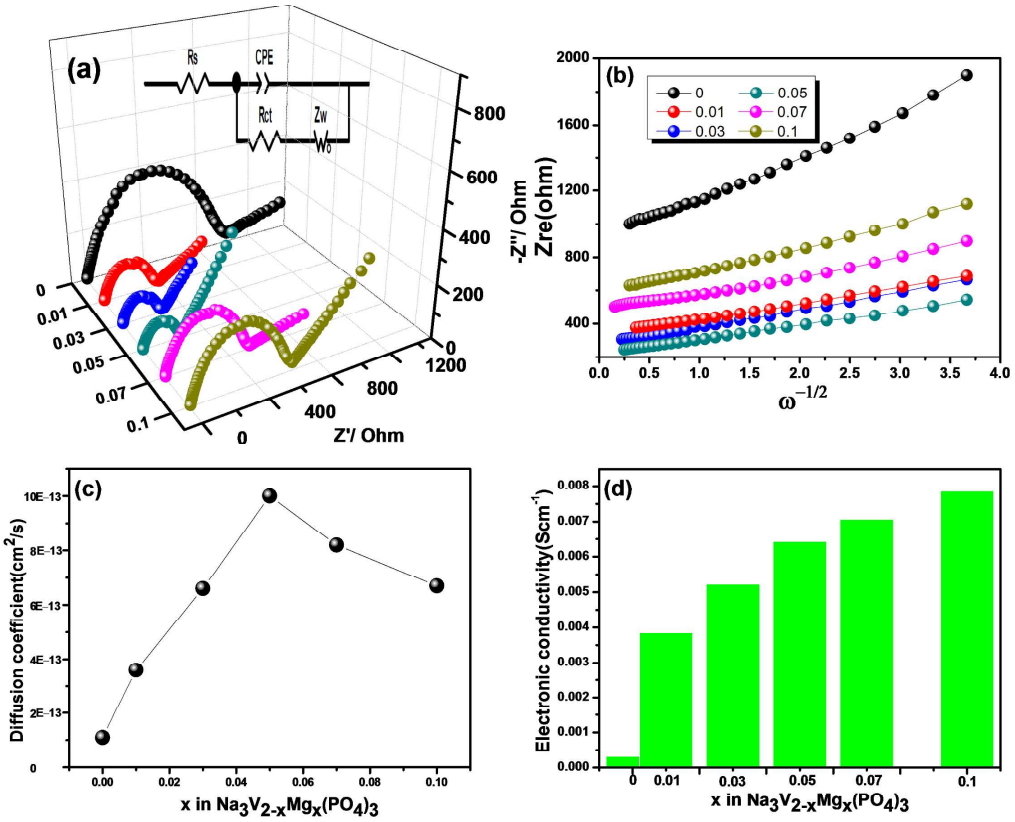

Fig. 4 a) Nyquist plots of the $Na_3V_{2-x}Mg_x(PO_4)_3$/C (x=0, 0.01, 0.03, 0.05, 0.07 and 0.1, inset: the equivalent circuit used to fit the EIS). b) The relationship between Zre and $\omega^{-1/2}$ at low frequencies. c) Sodium ion diffusion coefficients in $Na_3V_{2-x}Mg_x(PO_4)_3$/C (x=0, 0.01, 0.03, 0.05, 0.07 and 0.1). d) Electronic conductivity of $Na_3V_{2-x}Mg_x(PO_4)_3$/C (x=0, 0.01, 0.03, 0.05, 0.07 and 0.1), which was taken by a RTS-4 linear four-point probe measurement system

is charge transfer resistance. The Warburg impedance (Zw) represents the diffusion behavior at low frequency.[49] The fitting results of the equivalent circuit are listed in Table S7. Notably, the $Na_3V_{2-x}Mg_x(PO_4)_3$/C (x= 0.05) sample exhibits the smallest Rct (226.1 Ω), followed by x= 0.03, 0.01, 0.07, 0.1and 0, indicating the easier charge transfer for Mg doped materials. Furthermore, the diffusion coefficient (D_{Na^+}) of sodium ion can be calculated from the plots in the low-frequency region, and the equation can be expressed as[50,51]

$$D = \frac{R^2T^2}{2A^2n^4F^4C^2\sigma^2} \quad (1)$$

$$Z_{re} = R_e + R_{ct} + \sigma\omega^{1/2} \quad (2)$$

where R is the gas constant, T is the absolute temperature, A is the surface area of the cathode, n is the number of electrons per molecule during oxidization, F is the Faraday constant, C is the concentration of sodium ion(3.47×10^{-3} mol cm^{-3}), which can be calculated from the density and the molecular weight. σ is the Warburg factor which is relative with Zre(shown in reaction 2), ρ and M are the density and the molecular weight of the materials, respectively. Fig. 4b shows the relationship between Zre and square root of frequency ($\omega^{-1/2}$) in the low frequency region. A linear characteristic could be seen for every curve. The diffusion coefficient of sodium ion is calculated based on Eqs. (1) and (2). As demonstrated in Fig. 4c, the sodium ion diffusion coefficient of $Na_3V_{1.95}Mg_{0.05}(PO_4)_3$/C is 1.0×10^{-13} cm^2/s, an order higher than the undoped one($1.1\times10^{-14}cm^2/s$); and all the sodium ion diffusion coefficients of Mg doped $Na_3V_2(PO_4)_3$ are clearly higher than the undoped sample,

demonstrating that the rate of sodium diffusion in the charge/discharge processes is drastically increased by Mg^{2+} doping.

To explore the effects of doping on electronic conductivity, the electronic conductivity measurement was carried out using a RTS-4 linear four-point probe measurement system and the variation of electronic conductivity of $Na_3V_{2-x}Mg_x(PO_4)_3$ samples was shown in Fig. 4d. An increase in electronic conductivity is observed with the increase of Mg doping content. This is easy to understand. Mg^{2+} substitutes onto V site, in order to preserve the charge balance, there many holes, i.e., V^{4+}, will be generated. And then the conductivity increases. It is obvious that the increased sodium ion diffusion coefficients and electronic conductivity of $Na_3V_{2-x}Mg_x(PO_4)_3$(x=0.01, 0.03, 0.05, 0.07 and 0.1) will greatly improve the electrochemical performance, thus the observed superior rate capability as well as excellent cycling stability.

It is very interesting to point out that the variation trend of sodium ion diffusion coefficients of these $Na_3V_{2-x}Mg_x(PO_4)_3$ electrodes has an unexpected co-relationship with the variation of the electrochemical performance as shown in Fig. S4. Until recently, there is no clear evidence for the volcano-type variation in sodium ion diffusion coefficients, but the changes in lattice parameter with increasing doping level may lead to disruption of the Na^+ ion diffusion, as suggested by some previous studies.[52,53] From our results described above, it can be suggested that the volcano-type variation in the discharge capacity can be ascribed to several aspects: Firstly, the volcano-type variation of sodium ion diffusion coefficients lead to the same variation of discharge capacity. Secondly, since most of Mg^{2+} ions occupy the V site, in order to preserve the charge balance, many holes in valance band (associating with V^{4+}), will be generated, leading to the increase of electrical conductivity and thus improve the electrochemical performance.[54,55] Finally, Mg^{2+} is an inactive element in the materials, as discussed above, the theoretical specific capacity of $Na_3V_{2-x}Mg_x(PO_4)_3$ will decrease as a result of inactive magnesium element doped in the materials. Considering the effects of Mg doping, the different ionic conductivity and the increased electronic conductivity could be the major contributor to the improved electrochemical performance and rate capability of Mg doped $Na_3V_{1.95}Mg_{0.05}(PO_4)_3$/C.

Due to the lighter atomic weight, Mg is often considered as an ideal doping element. Chen[56] reported that Mg^{2+} doping in $LiFePO_4$ compound can improve the rate performance and cyclic stability of this material. Huang[57] demonstrated that the doping in V site by Mg^{2+} was favorable for the structural stability of $Li_3V_{2-x}Mg_x(PO_4)_3$/C and this led to an improved long term stability on cycling. However, studies on doping ion in $Na_3V_2(PO_4)_3$ have not been reported so far. Our experimental results show that a small amount of Mg doping does not significantly change the structure of the $Na_3V_2(PO_4)_3$ materials, but dramatically improve the electrochemical performance. The reasons can be attributed to the following aspects: firstly, by doping Mg into $Na_3V_2(PO_4)_3$, the morphology of smaller particle sizes can be obtained, which can increase the contact area between electrode and electrolyte, and accelerate the charge transfer between the interfaces. Secondly, in the case of V^{3+}, it will be changed to V^{4+} during the Na^+ extraction, which is smaller. As a result, the lattice will be contracted and limit the diffusion of sodium ions. In the Mg^{2+} doped sample, Mg^{2+} in the lattice could act as a pillar to prevent the collapse of the crystal during cycling. Hence, the existence of Mg^{2+} might be able to reduce the negative effects caused by the volume shrinking/swelling during the Na^+ extraction/insertion, resulting in increased cycle stability of Mg-doped $Na_3V_2(PO_4)_3$ system.[58,59] Thirdly, doping Mg into $Na_3V_2(PO_4)_3$ results in the lowered charge transfer resistance and increased sodium ion conductivity of $Na_3V_{2-x}Mg_x(PO_4)_3$(x=0.01, 0.03, 0.05, 0.07 and 0.1), helped in better electrochemical performance, including superior rate capability and excellent cycling stability. Finally, the existence of Mg^{2+} will cause some local defects in the

crystal structure, which might be able to increase the electronic conductivity, and hence improve the rate performance.

4 Conclusion

In summary, a series of Mg doped $Na_3V_{2-x}Mg_x(PO_4)_3$ (x=0, 0.01, 0.03, 0.05, 0.07 and 0.1) cathode materials were prepared by a sol-gel method. It has been found that the ionic and electronic conductivity of the $Na_3V_{2-x}Mg_x(PO_4)_3$ are significantly improved after Mg doping, resulting in dramatic improvement of the rate and cycle performances. For $Na_3V_{1.95}Mg_{0.05}(PO_4)_3$/C, when the cycling rate increased from 1 C to 30 C, the specific capacity only decreased from 112.5 mAh g^{-1} to 94.2 mAh g^{-1} demonstrating excellent rate capability. Moreover, even when cycled at high rate of 10 and 20 C, the initial capacity of 108.4 and 106.4 mAh g^{-1} can be obtained, and after 50 cycles, the discharge capacity can be stabilized at 104.6 and 86.2 mAh g^{-1} respectively. Such excellent electrochemistry performances in the $Na_3V_{1.95}Mg_{0.05}(PO_4)_3$/C containing earth abundant Mg and Na resources is very encouraging for the development of sodium ion batteries for industrial applications. In addition, These results demonstrate the advantages of using doping to increase the conductivity for other electrode materials of sodium ion batteries.

Acknowledgements

The present work is financially supported by National Basic Research Program of China (Grant No. 2015CB251100), Program for New Century Excellent Talents in University (Grant No. NCET-12-0047, NCET-13-0033). Y. Bai acknowledges the support from the State Scholarship Fund (No.201406035025) of the China Scholarship Council. The work done at Brookhaven National Laboratory was supported by the Assistant Secretary for Energy Efficiency and Renewable Energy, Office of Vehicle Technologies of the U.S. Department of Energy (DOE), under contact no. DE-AC02-98CH10886. The authors acknowledge the technique support by the beamline scientist at 9-BM-B of Advanced Photon Source at Argonne National Laboratory.

Notes and references

[a] Beijing Key Laboratory of Environmental Science and Engineering, School of Chemical Engineering and Environment, Beijing Institute of Technology, Beijing 100081, China. E-mail:membrane@bit.edu.cn(Y Bai); chuanwu@bit.edu.cn(C Wu)

[b] Chemistry Department, Brookhaven National Laboratory, Upton, New York 11973, USA.E-mail: xyang@bnl.gov (X.Q. Yang).

† Electronic Supplementary Information (ESI) available: SEM images of $Na_3V_{2-x}Mg_x(PO_4)_3$ (x = 0.01, 0.03, 0.07 and 0.1), EDS mapping images, conclusion of electrochemical data, XPS fitting parameters, results of structural analysis and crystallographic data obtained from XRD Rietveld refinement of samples $Na_3V_2(PO_4)_3$ and $Na_3V_{1.95}Mg_{0.05}(PO_4)_3$ and detailed EIS data. See DOI: 10.1039/b000000x/

1 V. Palomares, P. Serras, I. Villaluenga, K. B. Hueso, J. C. Gonzalez, T. Rojo, *Energy Environ. Sci.,* 2012, **5**, 5884.

2 M. S. Whittingham, *Chem. Rev*., 2004, **104**, 4271.

3 V. Etacheri, R. Marom, R. Elazari, G. Salitra, D. Aurbach, *Energy Environ. Sci.,* 2011, **4**, 3243.

4 F. Risacher, B. Fritz, *Aquat. Geochem.,* 2009, **15**, 123.

5 J. M. Tarascon, M. Armand, *Nature.,* 2001, **414**, 359.

6 W. E. Seyfried, D. R. Janecky, M. J. Mottl, Geochim. Cosmochim. Acta, 1984, **48**, 557.

7 P. Senguttuvan, G. Rousse, V. Seznec, J. M. Tarascon, M. R. Palacin, *Chem.Mater.,* 2011, **23**, 4109.

8 H. Li, C. Wu, F. Wu, Y. Bai, *Acta Chim. Sinica.,* 2014, **72**, 21.

9 J. Y. Jang, H. Kim, Y. W. Lee, K. T. Lee, K. Kang, N. S. Choi, *Electrochem.Commun.,* 2014, **44**, 74.

10 S. M. Oh, S. T. Myung, C. S. Yoon, J. Lu, J. Hassoun, B. Scrosati, K. Amine, Y. K. Sun, *Nano Lett.,* 2014, **14**, 1620.

11 S. M. Oh, S. T. Myung, J. Y. Hwang, B. Scrosati, K. Amine, Y. K. Sun, *Chem. Mater.,* 2014, **26**, 6165.

12 R. Berthelot, D.Carlier, C. Delmas, *Nat. Mater.,* 2011, **10**, 4.

13 L. Zhao, J. M. Zhao, Y. S. Hu, H. Li, Z. B. Zhou, M. Armand, L. Q. Chen, *Adv. Energy Mater.,* 2012, **2**, 962.

14 Y. U. Park, D. H. Seo, H. Kim, J. Kim, S. Lee, B. Kim, K. Kang, *Adv. Funct. Mater.,* 2014, **24**, 4603.

15 M. Pasta, C. D. Wessells, N. Liu, J. Nelson, M. T. McDowell, R. A. Huggins, M. F. Toney, Y. Cui, *Nat. Commun.,* 2014, **5**, 3007.

16 H. W. Lee, R. Y. Wang, M. Pasta, S. W. Lee, N. Liu, Y. Cui, *Nat. Commun*., 2014, **5**, 5280.

17 Y. J. Kim,Y. W. Park, A. Choi, *Adv. Mater.,* 2013, **25**, 3045.

18 J. F. Qian, X. Y. Wu, *Angew. Chem. Int. Ed.,* 2013, **52**, 4633.

19 K. T. Kim, G. Ali, K. Y. Chung, C. S. Yoon, H. Yashiro, Y. K. Sun, J. Lu, K. Amine, S. T. Myung, *Nano Lett.,* 2014, **14**, 416.

20 B. Dunn, H. Kamath, Jean. M. Tarascon, , 2011, **334**, 928.

21 F. Y. Cheng, J. Liang, Z. L. Tao, J. Chen, *Adv. Mater.,* 2011, **23**, 1695.

22 K. Saravanan, C. W. Mason, A. Rudola, K. H. Wong, P. Balaya, *Adv. Energy Mater.,*2013, **3**, 444.

23 W. Shen, C. Wang, H. M. Liu, W. S. Yang, *Chem. Eur. J.,* 2013, **19**, 14712.

24 C. B. Zhu, K. P. Song, P. A. V. Aken, Y. Yu, J. Maier, *Nano Lett.,* 2014, **14**, 2175.

25 S. Li , Y. F. Dong, L. Xu , X. Xu , L. He, L. Q. Mai, *Adv. Mater.,* 2014, **26**, 3545.

26 Z. L. Jian, L. Zhao, H. L. Pan, Y. S. Hu, H. Li, W. Chen. L. Q. Chen, *Electrochem.Commun.,* 2012, **14**, 86.

27 J.Gopalakrishnan, K. K. Rangan, *Chem. Mater.,* 1992, **4**, 745.

28 H. L. Fei. X. M. Wu, H. Li, M. D.Wei, *J Colloid Interf Sci.,* 2014, **415**, 85.

29 W. Wang, B. Jiang, L. W. Hu, Z. S. Lin, J. G. Hou, S. Q. Jiao, *J Power Sources,* 2014, **250**, 181.

30 Y. H. Jung, C. H. Lim, D. K. Kim, *J. Mater. Chem. A*, 2013, **1**, 11350.

31 J.Liu, K. Tang, K. P. Song, P. A. V. Aken, Y. Yu, J. Maier, *Nanoscale,*2014, **6**, 5081.

32 S. Y. Chung, J. T. Bloking, Y. M. Chinag, *Nat. Mater.* 2002, **1**, 122.

33 K. S.Park, P. Xiao, S. Y. Kim, A. Dylla, Y. M. Choi, G. Henkelman, K.J. Stevenson, J.B. Goodenough, *Chem. Mater.,* 2012, **24**, 3212.

34 B. Wang, B. H. Xu, T. F. Liu, P. Liu, *Nanoscale*, 2014, **6**, 986.

35 X. Yu, Y. C. Lyu, L. Gu, H. M. Wu, S. M. Bak, Y. N. Zhou, K. Amine, S. N. Ehrlich, H. Li, K. W. Nam, X. Q. Yang, *Adv. Energy Mater.,* 2014, **4**, 1300950.

36 S. Y. Chung, Y. M. Chiang, *Electro. Solid.ST,* 2003, **6**, A278.

37 N. Meethong, Y. H. Kao, S. A. Speakman, Y. M. Chiang, *Adv. Funct. Mater*., 2009, **19**, 1060.

38 J. Mendialdua, R. Casanova, Y. Barbaux, *J. Electron Spectrosc.,* 1995, **71**, 249.

39 Q. Kuang, Y. M. Zhao, X. N. An, J. M. Liu, Y. Z. Dong, L. Chen, *Electrochim. Acta,* 2010, **55**, 1575.

40 H. B. Shu, X. Y. Wang, Q. Wu, *J. Power Sources,* 2013, **237**, 149.

41 H. Zhang, Y. H. Tang, J. Q. Shen, *Appl. Phys. A,* 2011, **104**, 529.

42 H. B. Shu, X. Y. Wang, W. C. Wen, *Electrochim. Acta*, 2013, **89**, 479.

43 J. H. Yao, S. S. Wei, P. J. Zhang, C. Q. Shen, K. A. Zinsou, L. B. Wang, *J. Alloy. Compd.*, 2012, **532**, 49.

44 A. R. Cho, J. N. Son, V. Aravindan, H. Kim, K. S. Kang, W. S. Yoon, W. S. Kime, Y. S. Lee, *J. Mater. Chem.,* 2012, **22**, 6556.

45 T. Muraliganth, A. Vadivel Murugan, A. Manthiram, *Chem. Commun.,*2009, 7360.

46 Y. Ma , C. L. Fang , B. Ding , G. J, J. Y. Lee, *Adv. Mater.,* 2013, **25**, 4646.

47 E. Kang , Y. S. Jung, G. H. Kim, J. Chun, U. Wiesner, A. C. Dillon, J. K. Kim, J. Lee, *Adv. Funct. Mater.,* 2011, **21**, 4349.

48 X. Y. Wang, H. Hao, J. L. Liu, T. Huang, A. S.Yu, *Electrochim. Acta* ,2011, **56**, 4065.

49 S. Zhong, L. Wu, J. Liu, *Electrochim Acta*, 2012, **74**, 8.

50 H. Liu, Q. Cao, L.J. Fu, C. Li, Y. P. Wu, H. Q. Wu, *Electrochem. Commun.,* 2006, **8**, 1553.

51 H. Liu, C. Li, H. P. Zhang, L. J. Fu, Y. P. Wu, H. Q. Wu, *J. Power Sources,* 2006, **159**, 717.

52 H. Song, S. W. Yun, H. H. Chun, M. G. Kim, K. Y. Chung, H. S. Kim, B. W. Chod, Y. T. Kim, *Energy Environ. Sci.,* 2012, **5**, 9903.

53 K. M. Shaju, G. V. Subba Rao, B. V. R. Chowdari, *J. Mater. Chem.,* 2003, **13**, 106.

54 Y. Z. Dong, Y. M. Zhao. H. Duan, *J. Electroanal. Chem*, 2011, **660**, 14.

55 H. Tukamoto, A. R. West, *J. Electrochem. Soc*, 1997, **144**, 3164.

56 D. Y. Wang, H. Li, S. Q. Shi, X. J. Huang, L. Q. Chen, *Electrochim. Acta*, 2005, **50**, 2955.

57 J. S. Huang, L. Yang, K.Y. Liu, Y. F. Tang, *J. Power Sources,* 2010, **195**, 5013.

58 J. S. Huang, L. Yang, K.Y. Liu, Y. F. Tang, *J Power Sources*, 2010, **195**, 5013.

59 M. M. Ren, Z. Zhou, Y. Z. Li, X. P. Gao, J. Yan, *J Power Sources*, 2006, **162**, 1357.

60 W. Shen, C. Wang, Q. J. Xu, H. M. Liu, Y. G. Wang, *Adv. EnergyMater.,* 2014, 1400982.

61 G. Q. Li, D. L. Jiang, H. Wang, X. Z. Lan, H. H. Zhong, Y. Jiang, *J. Power Sources,* 2014, **265**, 325.